Blood Cells, Molecules and Diseases 75 (2019) 1–10

Contents lists available at ScienceDirect

Blood Cells, Molecules and Diseases

journal homepage: www.elsevier.com/locate/bcmd

Primary CNS lymphoma patient-derived orthotopic xenograft model capture the biological and molecular characteristics of the disease

Frédéric Pouzoulet[a,1], Agusti Alentorn[b,c,1], Louis Royer-Perron[c], Franck Assayag[a], Karima Mokhtari[d], Dalila Labiod[a], Magali Le Garff-Tavernier[e,f], Mailys Daniau[c], Emmanuelle Menet[g], Matthieu Peyre[h], Anne Schnitzler[i], Justine Guegan[c], Frédéric Davi[e], Khê Hoang-Xuan[b], Carole Soussain[j,*]

[a] Experimental Radiotherapy Platform, Translationnal Research Department, Institut Curie, Orsay, France
[b] Groupe Hospitalier Pitié-Salpétrière, Neuro-oncology, Paris, France
[c] Paris University Sorbonne UPMC, INSERM U1127, CNRS UMR 7225, IHU, ICM, France
[d] Groupe Hospitalier Pitié-Salpétrière, Neuro-Pathology, Paris, France
[e] Groupe Hospitalier Pitié-Salpétrière, Biological Hematology, Paris, France
[f] Paris University Sorbonne UPMC, INSERM UMRS 1138, Paris, France
[g] Institut Curie, Pathology, Site Saint-Cloud, France
[h] Groupe Hospitalier Pitié-Salpétrière, Neurosurgery, Paris, France
[i] Institut Curie, Site Paris, Pharmacogenomics Unit, Genetics Department, Paris, France
[j] Institut Curie, Site Saint-Cloud Hematology, Saint-Cloud, France

ARTICLE INFO

Editor: Mohandas Narla

ABSTRACT

Primary CNS lymphomas (PCNSL) are rare and poor prognosis diffuse large B-cell lymphomas. Because of the brain tumor environment and the restricted distribution of drugs in the CNS, specific PCNSL patient-derived orthotopic xenograft (PDOX) models are needed for preclinical research to improve the prognosis of PCNSL patients. PCNSL patient specimens (n = 6) were grafted in the caudate nucleus of immunodeficient nude mice with a 83% rate of success, while subcutaneous implantation in nude mice of human PCNSL sample did not generate lymphoma, supporting the role of the brain microenvironment in the PCNSL physiopathology. PDOXs showed diffuse infiltration of B-cell lymphoma cells in the brain parenchyma. Each model had a unique mutational signature for genes in the BCR and NF-κB pathways and retained the mutational profile of the primary tumor. The models can be stored as cryopreserved biobank. Human IL-10 levels measured in the plasma of PCNSL-PDOX mice showed to be a reliable tool to monitor the tumor burden. Treatment response could be measured after a short treatment with the targeted therapy ibrutinib. In summary, we established a panel of human PCNSL-PDOX models that capture the histological and molecular characteristics of the disease and that proved suitable for preclinical experiments. Our methods of generation and characterization will enable the generation of additional PDOX-PCNSL models, essential tools for cognitive and preclinical drug discovery.

1. Introduction

Primary central nervous system lymphomas (PCNSLs) are a rare form of diffuse large B-cell lymphoma (DLBCL) with a poor prognosis. There have been considerable efforts to unravel the biology of PCNSL, which has been less studied than systemic lymphoma, mainly because of the lack of available material from stereotaxic biopsies and the rarity of the disease. PCNSL is unusual in that it is confined to the CNS, an area normally devoid of B-cells. PCNSLs are mainly DLBCLs of an activated B-cell-like (ABC) subtype [1,2]. Improvement in molecular techniques has led to a better molecular characterization of this disease. PCNSL harbors mutations in *MYD88* and *CD79B*, as does nodal ABC-DLBCL, but the pattern is more consistent: these mutations are found in 30 to 80% of patients according to previous studies [3,4]. PCNSL exhibits B-cell receptor (BCR) activation, BCL6 deregulation and NF-κB pathway activation. Other genomic abnormalities have been found, such as 6p21.32 loss (HLA locus), 6q loss, *CDKN2A* homozygous deletions, and frequent PD-L1 deregulation [4]. Similar to nodal DLBCL, the

* Corresponding author at: Hematology, Institut Curie, Site Saint-Cloud, 35 rue Dailly, 92210 Saint-Cloud, France.
E-mail address: carole.soussain@curie.fr (C. Soussain).
[1] These two authors contributed equally to the work.

https://doi.org/10.1016/j.bcmd.2018.11.005
Received 14 November 2018; Accepted 15 November 2018
Available online 16 November 2018
1079-9796/

responses of PCNSL to standard treatments are heterogeneous. In PCNSL, the brain tumor environment appears to be involved in the mechanisms underlying the cerebral tropism of this type of lymphoma [5,6]. Treatment efficacy also depends on drug bioavailability in the brain parenchyma [7].

Despite the molecular heterogeneity of PCNSL, the empirically determined first-line treatment relies on high-dose methotrexate-based chemotherapy. However, the complete remission rate after such induction chemotherapy remains below 50% [8,9].

Findings regarding responses of nodal lymphomas to innovative drugs cannot be directly translated to PCNSL patients in clinical practice. Preclinical models that mimic the molecular characteristics and functional heterogeneity of PCNSL are needed for cognitive and preclinical research purposes. No bank of PCNSL patient-derived xenograft (PDOX) models has been published to date. Accordingly, no primary PCNSL cell lines are commercially available.

We present a platform for the development and the characterization of patient derived PCNSL orthotopic (PCNSL-PDOX) models that mimic the biological and molecular characteristics of the patient disease. The PCNS-PDOX can be frozen for storage and are suitable for preclinical experiment.

2. Results

2.1. Establishment of PDOX models

We obtained 6 samples: 3 fresh biopsy samples from patients undergoing diagnostic cerebral biopsy and 3 cerebrospinal fluid (CSF) samples from patients undergoing lumbar puncture for CSF analysis during the disease work-up at relapse (Table 1). All the patients had DLBCL PCNSL (n = 5) or large B-cell lymphoma primary vitreoretinal lymphoma (PVRL) (n = 1). The orthotopic implantation of these tumor samples in the mice brain was successful in 5 cases, resulting in an initial engraftment rate of 83% (5/6). In one case (CSF-1), the model could not be maintained because the mouse died without any warning. Stable PDOX–PCNSL models were established from the other 4 samples. Additional CSF was collected from a PCNSL patient with no CSF involvement and implanted in mice to serve as a negative control to rule out the development of murine lymphoma. Pathological examination of the brain was performed at each passage of the PDOX. The DLBCL diagnosis was confirmed on all mouse brain samples (Fig. 1). Perivascular tropism was characteristic. Two PDOXs had non-GC IHC profiles according to the Hans algorithm [10] (negative for CD10 and positive for Bcl6 and MUM1), and the 2 other PDOX models were positive for both CD10 and MUM1. Double CD10 and MUM1 positive DLBCL emerged as a subgroup with a similar OS and PFS to those of non-GC DLBCL [11]. The IHC results of the PDOX models matched the results of the corresponding primary tumor, except for an aberrant MUM1-positive finding in PDOX-BDB2 (Table 1). The EBV status was negative in the patient samples and PDOX models (Table 1).

2.2. Growth parameters of PCNSL-PDOX models

The rate of tumor engraftment at passage 0 (first passage from patient to animal) was 33% to 100%, and this rate increased steadily upon passages to reach 70–100% engraftment (Table 2).

The latency, defined as the time from implantation to the first endpoint, was also stable over time, with an average of 58 days (range, 40 to 93 days) for the 5 models and until passage 5.

2.3. Specificity of the brain microenvironment

A fresh fragment of the BDB-1 model was inoculated subcutaneously and in the mammary fat-pad in two groups of 3 mice. No tumor graft was observed neither locally, nor at distance of the site of implantation, supporting the role of the brain microenvironment in PCNSL.

2.4. Frozen bank of PDOX models

For ethical reasons and to avoid the cost of maintaining a live mouse tumor bank, we performed thawing tests on the four PDOX models at early passage after the samples were stored for than three months in liquid nitrogen; the tests were successful in all cases (Table 2).

2.5. Molecular characteristics of the PDOX models and comparative analysis with the initial tumors

The mutational profiles of the 4 PDOX models were determined and compared with those of the original patient sample in 3 cases. PDOX-LCR4 was obtained from a patient with an initial diagnosis of PVRL and relapses in the eye and CSF. Since the initial diagnosis was made by examination of the vitreous, no biopsy sample was available.

We performed three paired (tumor and PDOX) NGS analyses of a targeted panel of approximately 100 genes recurrently mutated in PCNSL/DLBCL. The four models exhibited 4 distinct mutational profiles regarding *CD79A*, *CD79B*, *PIM1*, *CARD11*, and *TBL1XR1*, which are involved in the BCR and NF-κB pathways; these profiles matched those of the primary tumors (Table 3).

In addition, we analyzed the transcriptome of paired tumor/PDOX samples by RNA-seq analysis. Variant allele frequency and clonotype profiling were highly similar between early passage PDOX models and primary tumors. Late passage PDOX models showed a hypermutated genotype compared to primary tumor and early passage samples (Fig. 2), as well as a selected clonotype profile, and some mutations were exclusive to PDOX samples.

Primary tumors and corresponding PDOX models showed a similar ABC transcriptomic profile (Fig. 3).

2.6. B-cell origin and clonal rearrangement of IGH

The B-cell repertoire was also analyzed using RNA-seq data. We analyzed two pairs of PDOX models/primary tumors (Fig. 4). The clonotype of the early passage PDOX was similar to that of the primary

Table 1
Pathology and immunohistochemistry of PDOX models and their corresponding primary tumors.

	Origin	Histology	Ki67	CD20	CD10	BCL6	MUM1	EBER
PDOX-BDB1	PCNSL at diagnosis	DLBCL	100%	+	−	+	+	−
Primary tumor BDB-1		DLBCL	90%	+	−	+	+	−
PDOX-BDB2	PCNSL at diagnosis	DLBCL	100%	+	+	+	+	−
Primary tumor BDB-2		DLBCL	90%	+	+	+	−	−
PDOX-CSF-3	PCNSL at relapse	DLBCL	100%	+	−	+	+	−
Primary tumor CSF-3		DLBCL	NA	NA	−	NA	NA	NA
PDOX-CSF-4	PCNSL at relapse	DLBCL	100%	+	+ + +	NA	+	−
Primary tumor CSF-4		DLBCL	NA	NA	+	NA	NA	NA

NA: non available; positivity for CD20, CD10, BLC6 and MUM1 was defined as at ≥30% positive cells.

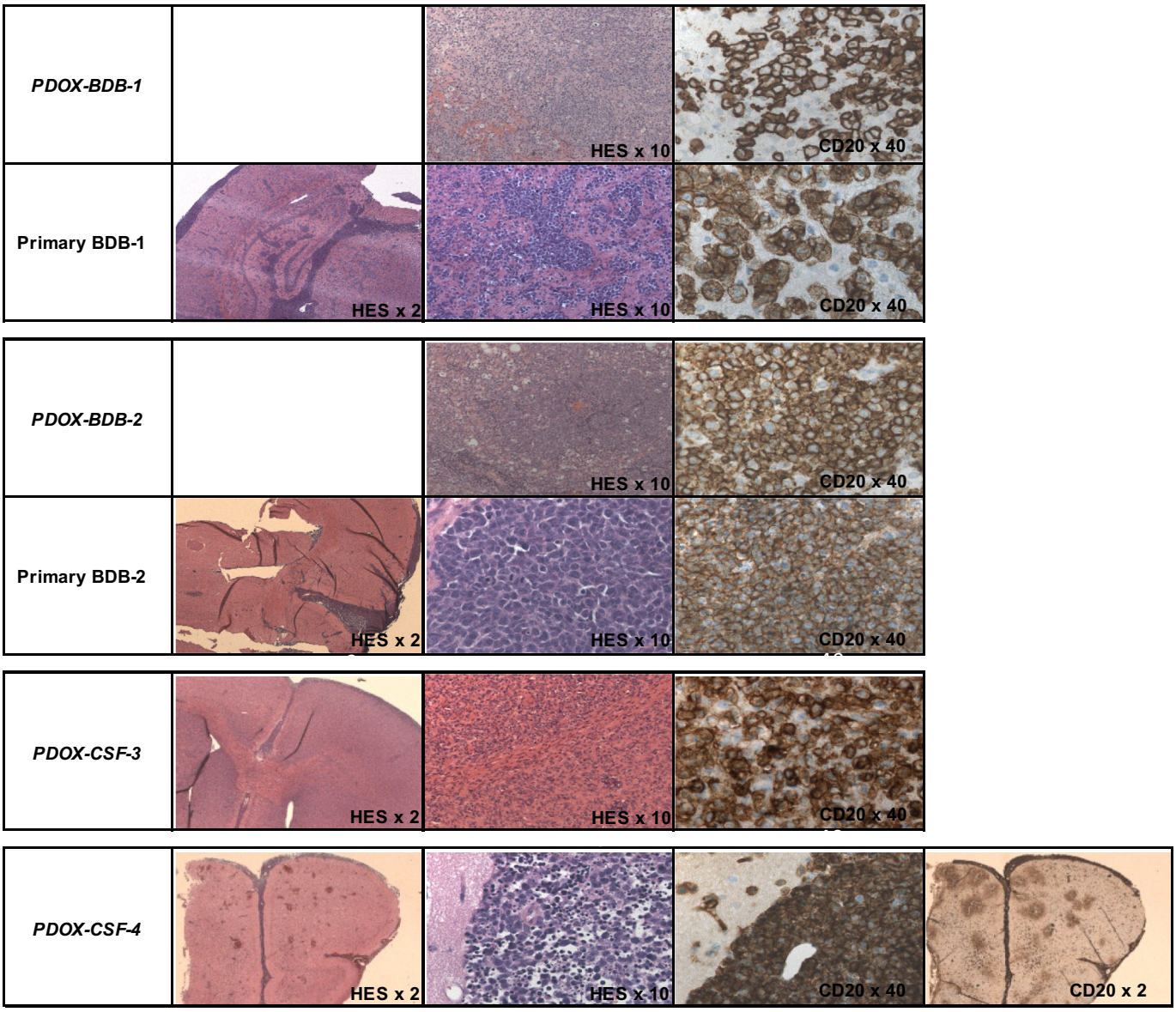

Fig. 1. Histology of PDOX models and their corresponding primary tumors.

Table 2
PDOX growth parameters.

	Engraftment rate (%) at p0	Mean survival at p0 (days)	Last passage	Engraftment rate (%) after thawing
PDOX-BDB-1	33%	48	p14	90%
PDOX-BDB-2	50%	60	P7	20%
PDOX-CSF-3	100%	67	p4	40%
PDOX-CSF-4	50%	93	P4	100%

tumor but was highly selected in the late passage PDOX.

2.7. Tumor growth monitoring by qPCR-based quantification of tumor cell content and correlation between IL-10 plasma levels and tumor burden

To optimize the preclinical and cognitive use of these PDOX models, we sought a quantitative method to monitor tumor growth.

Tumor grafts led to diffuse infiltration of the brain parenchyma within 30 to 90 days. The human cell load (defined as the percentage of human cells versus murine cells), which was quantified in the mouse brain by qPCR, was 32% at the ethical endpoint for PDOX-BDB1.

IL-10 was used as a marker of DLBCL-PCNSL as previously described [12]. Human IL-10 was undetectable in mice before implantation of the

Table 3
Molecular diversity of the PCNSL models and a comparison of mutational profiles between primary tumors and associated PDOX models (the CSF-4 primary tumor sample was not available).

	MYD88	*CD79A*	*CD79B*	*PIM1*	*CARD11*	*TBL1XR1*
PDOX-BDB1	L265P	WT	p.Y196H	p.S146R	WT	WT
Primary tumor BDB-1	L265P	WT	p.Y196H	p.S146R	WT	WT
PDOX-BDB2	WT	p.V64I	p.Y196H	WT	WT	WT
Primary tumor BDB-2	WT	p.V64I	p.Y196H	WT	WT	WT
PDOX-CSF-3	L265P		p.Y196H			WT
Primary tumor CSF-3	L265P		p.Y196H	p.P33S		WT
PDOX-CSF-4	L265P		p.Y196H	p.S59A		p.S419F
Primary tumor CSF-4						

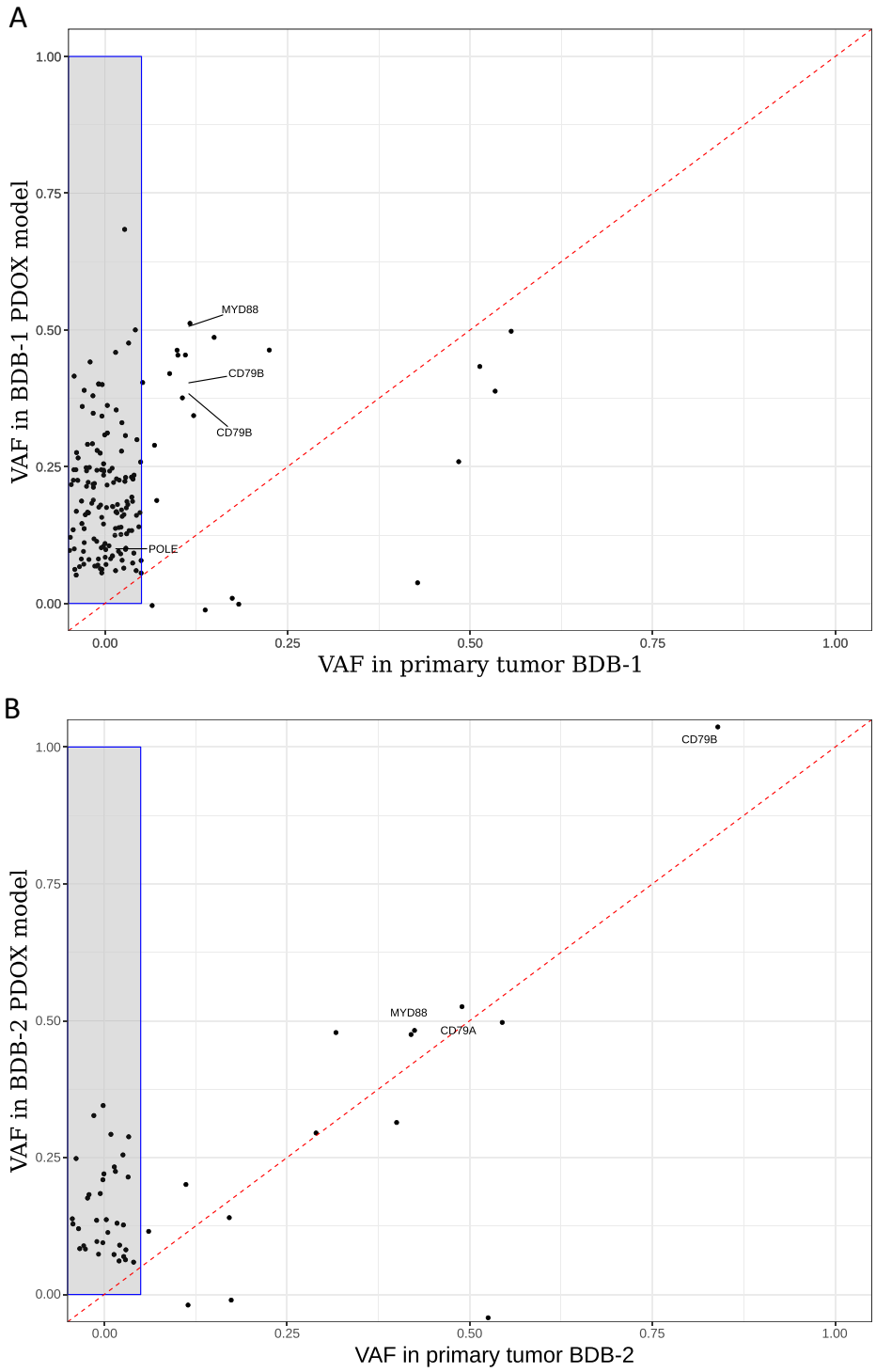

Fig. 2. Comparison of variant allele frequency (VAF) of somatic mutations between the primary tumor (patient source on x axis) and the corresponding PDOX model (y-axis). Identical VAF values between the primary tumor and PDOX model are indicated by the red dotted line. Mutations exclusive to the PDOX model are found in the gray area. The analyses were performed on passage 7 of the BDB-1 PDOX model (A) and on the first passage of the BDB-2 PDOX model (B). The BDB-1 PDOX model at passage 7 showed a hypermutation phenotype with mutations of the POLE gene and different mismatch-repair genes. (For interpretation of the references to colour in this figure legend, the reader is referred to the web version of this article.)

human PCNSL samples. Serial blood measures of human IL-10 were performed in the PDOX-BDB-1 model, along with pathological examination and tumor cell load quantification. Human IL-10 levels increased after tumor implantation (Fig. 5A), and IL-10 level correlated with tumor cell load (Fig. 5B).

2.8. Feasibility of preclinical experiments on PCNSL PDOX model

The BDB-2 model was used for this experiment. The Bruton-tyrosine kinase (BTK) inhibitor, ibrutinib was chosen as a targeted therapy interfering in the BCR pathway. The treatment response could be assessed after a short treatment by ibrutinib by the size of the tumor on brain slices and by the plasma IL-10 levels. Tumoral infiltration was smaller in the ibrutinib-treated mice than in control animals as illustrated in Fig. 6A. After treatment, the serum IL-10 level increased in the control mice, and decreased after ibrutinib-treated mice (Table 4).

3. Discussion

PDOX models of PCNSL are needed to conduct studies with the goal of improving the outcome of PCNSL patients. The rarity of this disease limits the ability to rapidly conduct early clinical trials, while an

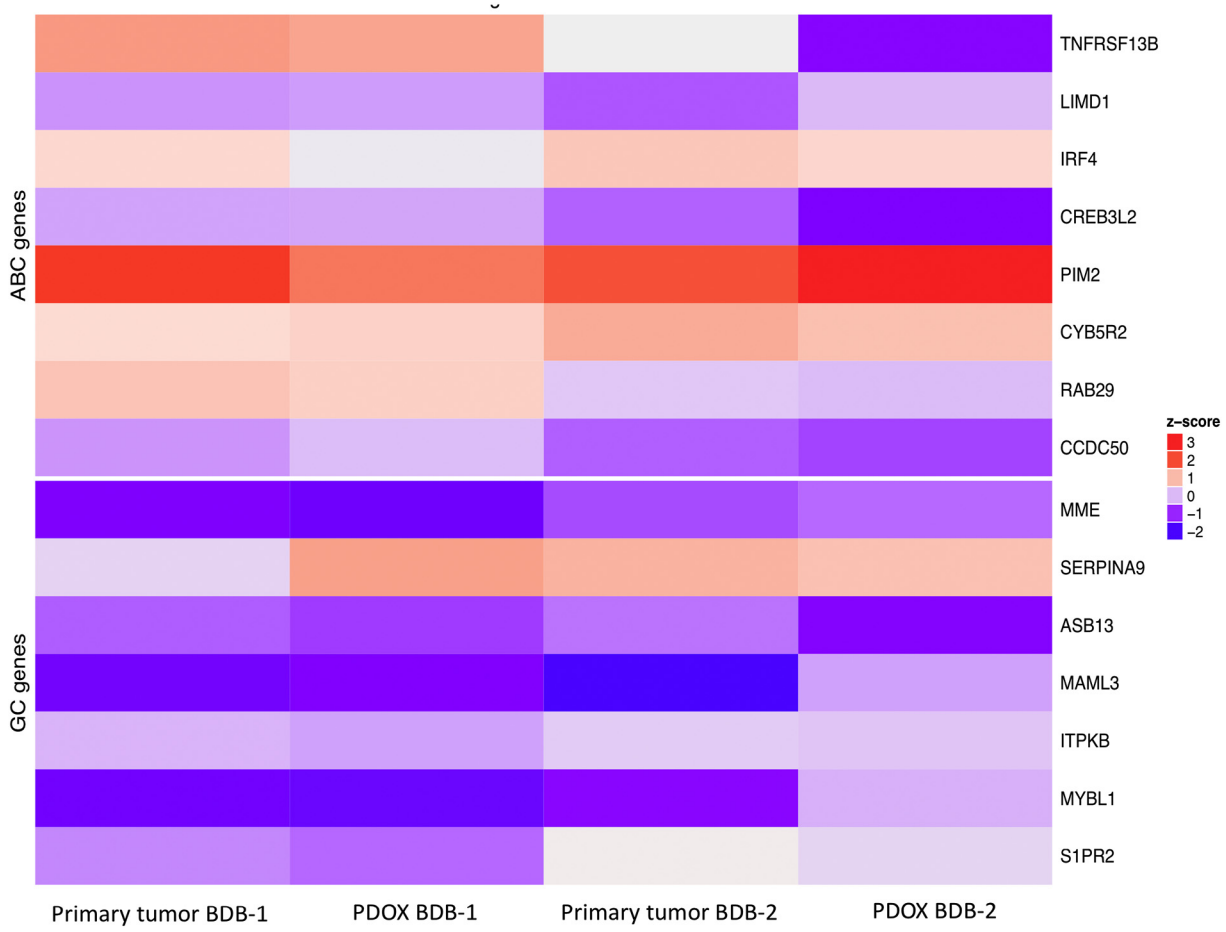

Fig. 3. Activated B-cell and Germinal center transcriptome signatures in primary tumors and associated PDOX models using a heatmap representation of z-scores.

increasing number of targeted therapies and immunotherapies are available for DLBCL. These therapies must be tested alone or in combination in the specific setting of PCNSL due to the impact of the specific localization of the disease in the brain on the treatment response. Molecular studies in PCNSL patients have revealed similar patterns of molecular characteristics as those in nodal DLBCL of the non-GC subtype but have also suggested different mutation frequencies and specificities linked to the brain micro-environment.

Grommes et al. [13] generated two PCNSL-PDOX models from *CD79B*-mutant PCNSL biopsy samples that were enzymatically treated, which were used for ex-vivo experiments. To our knowledge, our study is the first one describing the generation of a panel of multiple human PCNSL-PDOX models that capture the histological and molecular characteristics of the disease with a steady engraftment rate, following a reliable and reproducible pattern of characterization. Our PDOX models retain the main molecular characteristics of the primary tumor, especially regarding *MYD88*, *CD79* and *CARD11* mutations and their non-GC transcriptome profile [4]. Although the transcriptome results were consistent with a non-GC profile in the 4 cases, the mutational profile was heterogeneous. Indeed, the 4 PDOX models showed a different combination of *MYD88*, *CD79A*, *CD79B*, *PIM1* and *TBL1XR1* mutations. As described in multiple PDOX models [14], late passages show clonal selection relative to the primary tumor and the emergence of alterations in the mouse genome. We showed that the average engraftment rate increased with passage number, indicating possible tumor adaptation to the murine host. This clonal selection in mice could be avoided by storing early passage samples. On the other hand, this clonal selection could be useful for testing selected targeted therapies.

PCNSL-PDOX models are also suitable for experiments with immunotherapies. Indeed, the nude mice lack T-cells but have normal microglia cells, therefore a normal innate immune system including NK cells. These features allow studies on the role of innate immunity and studies using CART cells, as they will not be rejected by mouse T cells. CART-cells have been tested in models of lymphoma using nod scid gamma mice, which lack B, T and NK cells [15,16].

For these models to be applicable in preclinical studies, a surrogate marker of tumor engraftment is required. The image resolution of the MRI in mice is low and luciferase transfection cannot be performed on fresh and cryopreserved tumor samples before implantation. To circumvent this challenge, we showed that human IL-10 levels in murine plasma can be used as a surrogate maker of tumor engraftment, tumor growth, and therapeutic response, in IL-10 secreting tumors. Should the tumor not secrete IL-10, other approaches have to be developed such as imaging techniques or detection of circulating cell-free human DNA. Beta-2 microglobuline has been used as a surrogate marker of tumor burden in peripheral lymphoma PDX [17], but this biomarker has not been validated yet in PCNSL. The PDOX models are viable for an average of 62 days, making them convenient for drug screening.

The PDOX models can be cryopreserved, thus eliminating the need to maintain live animals.

4. Conclusions

We developed 4 PCNSL-PDOX models with fresh and cryopreserved material that recapitulate the molecular characteristics of the primary tumors and the heterogeneity of the disease. These models are suitable for preclinical studies, drug screening and cognitive research. Additional models are currently under development following the same pattern of characterization.

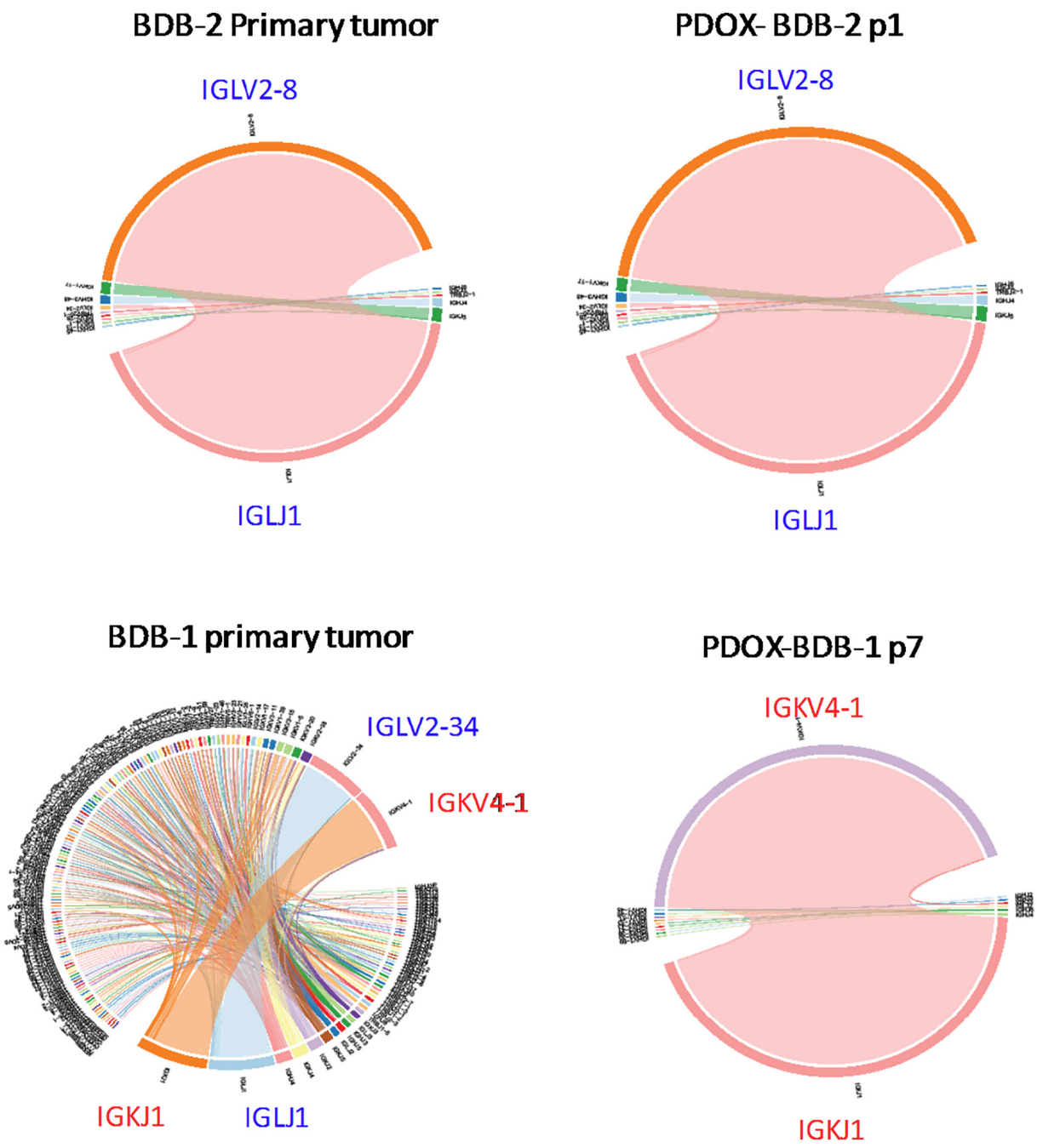

Fig. 4. V-J junction circos plots for primary tumors and their corresponding PDOX models. Arcs correspond to different V and J segments and are scaled to their frequency in the sample. Ribbons represent V-J pairing, and their size is scaled to the pairing frequency.
The V-J circos junction plots for BDB-2 PDOX at passage 1 and the primary tumor show a highly similar clonotype, while those for BDB-1 at passage 7 and its primary tumor show a selected clonotype.

5. Materials and methods

5.1. Patient tumor samples

Fresh samples of remnants of the brain diagnostic biopsy (BDB) or of cerebrospinal fluid (CSF) were collected from adult immunocompetent patients at Hôpital Pitié-Salpétrière and Institut Curie. All patients had previously provided informed consent for use of their samples for research purposes.

5.2. Animals

Six-week-old immunodeficient nude mice (Charles River Laboratories, France) were used to establish PDOX models. Mice were maintained in a specific pathogen-free environment and were observed daily for clinical signs (ataxia, cachexia, and behavioral changes) and weight loss.

5.3. Establishment of PDOX models

Patient specimens were transported at 4 °C in Iscove's Modified Dulbecco's Medium (IMDM; Sigma-Aldrich) supplemented with 20%

A. Kinetic of plasmatic human IL-10 levels in one BDB-1 mouse over time after implantation.

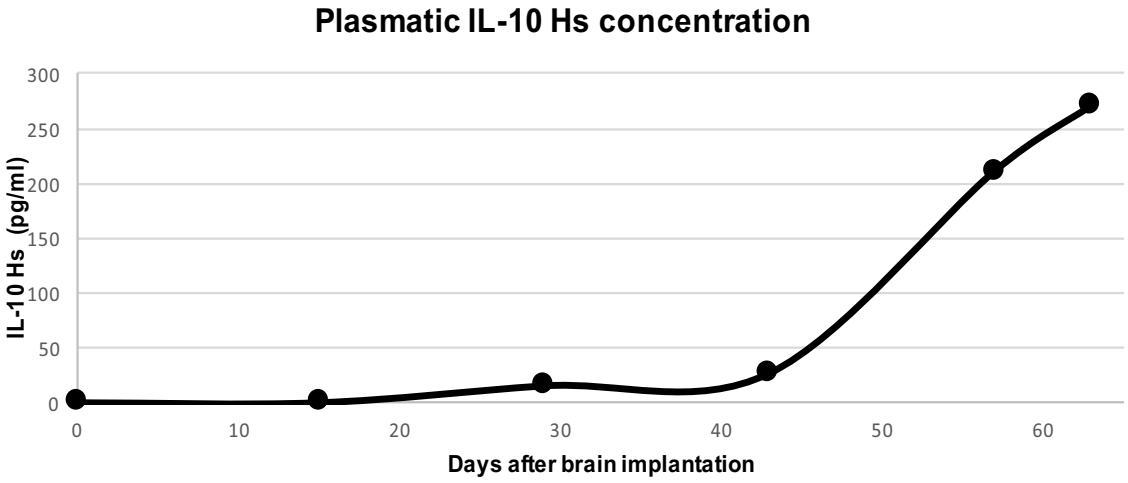

B. Correlation between Human cell load and plasma IL-10 levels in BDB-1 PDOX mice. Blood samples were obtained every15 days and at the time of sacrifice.

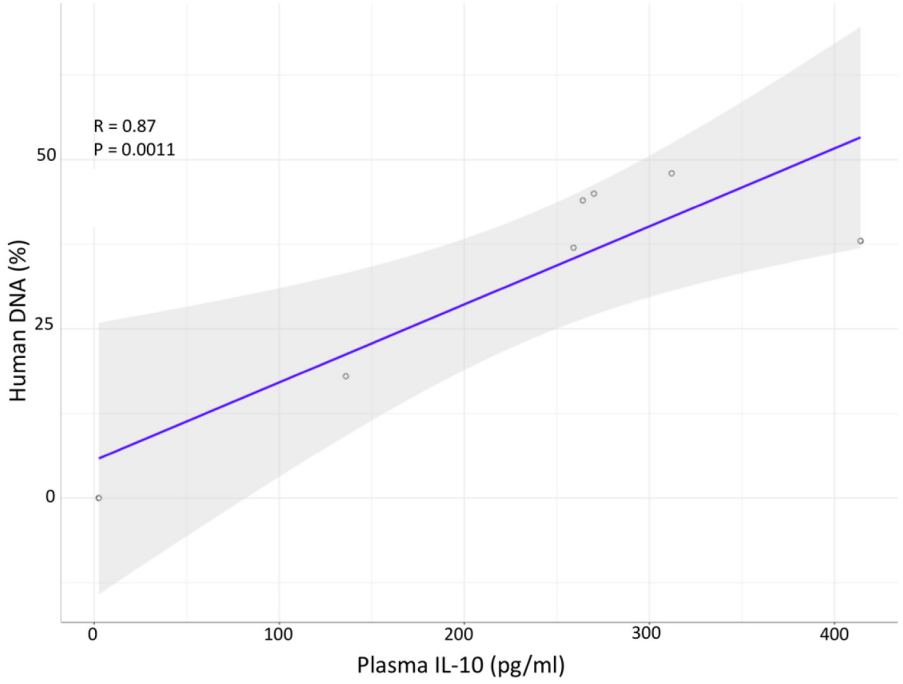

Fig. 5. Human IL-10 level in mice plasma.
A. Kinetic of plasmatic human IL-10 levels in one BDB-1 mouse over time after implantation.
B. Correlation between Human cell load and plasma IL-10 levels in BDB-1 PDOX mice. Blood samples were obtained every15 days and at the time of sacrifice.

fetal bovine serum (FBS; Biowest) and 1% penicillin/streptomycin antibiotics (P/S; Gibco). Fresh biopsy tumor samples were mechanically dissociated. CSF cells were counted, checked for viability, concentrated and then resuspended in 5 µl of phosphate-buffered saline. The CSF or BDB biopsies were then injected into the right striatum of the mice without additional manipulation of the cells. The endpoints for tumor engraftment included weight loss, clinical signs of ataxia, and cranial deformation, and scored according to a scale validated by the ethic committee for animal experimentation of Institut Curie (Table 5). When one of these endpoints was observed, the mouse was sacrificed, and the brain was removed. The part of the brain corresponding to the site of tumor implantation was dissected, extracted and re-implanted in other mice. Tissue passaging was repeated to check the viability and graft rate of each PDOX. Fresh material was preserved in 10% DMSO + 90% FBS

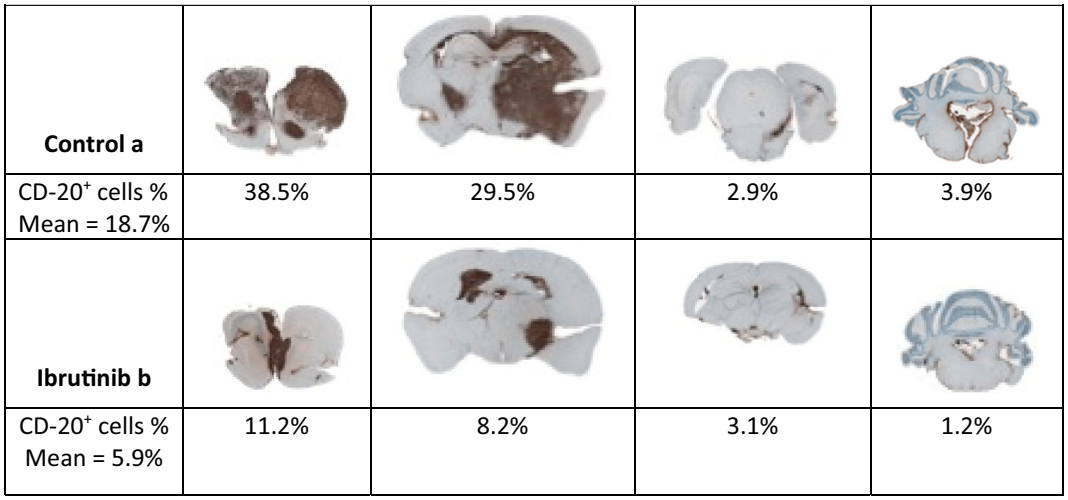

Fig. 6. Illustration of the effect of a short treatment with ibrutinib in the BDB-2 model. Mice with BDB-2 PCNSL-PDOX tumors were treated with Ibrutinib (30 mg/kg/day, tube feeding) for 5 days from day 49 after implantation (n = 3), or by vehicle (n = 3). Mice were sacrificed 4 h after last treatment intake on day 56. Quantification of the percentage of CD-20+ cells/total cells was performed on the four brain slices.

Table 4
Peripheral human IL-10 level before treatment and after treatment in all mice.

	Peripheral human IL 10 level pg/ml	
	Pre-treatment	Post-treatment
Control a	2.89	3.32
Control b	Undetectable	3.61
Control c	Undetectable	2.74
Ibrutinib a	3.61	Undetectable
Ibrutinib b	3.39	Undetectable
Ibrutinib c	2.6	Undetectable

Table 5
Scoring system for clinical follow-up of mice.

Symptoms −: present (+) doubtful (±) absent (−)	
If 4 minor criteria (a) or 1 major criterion (b) are met (+), the animal is sacrificed.	
Outside appearance	
Self-injury	(a)
Abdominal distension	(a)
Arched back	(a)
Feces: blood/diarrhea	(a)
Isolation/prostration	(a)
Pallor (eyes, ears, skin, pads): hematopoietic symptoms	(a)
Slow or difficult breathing	(a)
Cachexia	(b)
Deformation of the skull	(b)
Postoperative motor disorders (appearance in the postoperative week)	(b)
Weight loss > 20%	(b)
Reduced mobility (Incoordination, tremors, paralysis)	(b)
Reaction to the manipulation	
Reluctant to move	(a)

in liquid nitrogen.

At the time of sacrifice, mice were clinically examined to rule out any lymphoma spread outside the brain.

5.4. Histopathology of patient samples and xenograft brains

Pathological analyses of paraffin-embedded sections of patient samples and mouse brain were performed according to standard protocols, and immunohistochemistry (IHC) analyses were conducted to evaluate CD20, CD10, CD3, BCL6, MUM1, EBER and Ki67 expression.

5.5. Mutational profiles, RNA-seq, VDJ recombination, and CapLoc

5.5.1. Nucleic acid extraction

Tumor DNA was extracted with a QIAamp DNA Mini Kit. Plasma DNA was extracted with a Qiagen QIAamp® Circulating Nuclear Acid Kit according to the manufacturer's protocol.

Tumor DNA quantity and quality were evaluated with a Thermo Scientific NanoDrop™ 8000. An Agilent TapeStation system was then used for quality control, with High Sensitivity D1000 ScreenTape for plasma DNA and Genomic DNA ScreenTape for tumor DNA.

Total RNA was extracted from cryopreserved samples using the iPrep Trizol® Plus RNA Kit (Life Technologies). Enrichment and capture were performed using a custom Roche SeqCap EZ system. We chose the most frequently mutated genes within a targeted sequencing panel of 500 kb. Sequencing was performed on an Illumina NextSeq system.

The RNA-seq library was prepared using the TruSeq Stranded mRNA Kit protocol (Illumina) with an input of 500 ng of total RNA. Polyadenylated RNA was captured using oligo dT beads. Captured RNA was fragmented into pieces of approximately 400 bp. After DNA synthesis, Illumina adaptor ligation, library amplification by PCR, and 100-bp paired-end sequencing were performed using the Illumina NextSeq system.

5.5.2. Bioinformatics

Trimmomatic v0.36 was used to filter and trim poor-quality reads [18]. DNA alignment was performed using bwa v0.7.15 (using default values) on the hg19 human genome build. Variant calling (single nucleotide variants and insertions/deletions) was performed using the GATK (v3.6) pipeline for the selected gene panel analyzed by targeted sequencing [19]. Quantitative data on coverage and on/off-target reads were obtained using Picard Tools (http://broadinstitute.github.io/picard/). Variant annotation was analyzed using ANNOVAR [20]. Further data annotation was performed with Oncotator [21]. Data were visualized with the maftools package in R [22].

Raw RNA-seq data were pseudo-aligned using kallisto v0.43.1 using GRCh37 v75 of the human transcriptome [23]. Transcript abundance is presented in transcripts per million (TPM).

We also extracted T-cell receptor (TCR) and BCR CDR3 repertoires from RNA-seq data using MiXCR [24]. We preserved partial alignments (-OallPartialAlignments = true) and performed two iterations of reads using mixcr assemblePartial. Finally, we extended TCR alignments with uniquely determined V and J genes having incomplete coverage of CDR3q using germline sequences, and we assembled the results using

the mixcr assemble function. The results were visualized using VDJtools [25].

5.5.3. Quantification of tumor grafts

PDOX tumor mass was evaluated by quantifying human cells in mouse brains by qPCR analysis. The DNA copy number of specific human genes (i.e., ALB) and of both mouse and human genes (i.e., JUN) was quantified by real-time quantitative PCR to determine the quantity of human tumor cells in PDOX tissues. With assistance from the computer program Oligo 6.0 (National Biosciences, Plymouth, MN, USA), the human Alb primer pair was selected to be human specific by comparison with the murine alb gene sequence, whereas the Total-JUN primer pair was selected to amplify both the mouse and human JUN genes. BLASTN searches against nr (the non-redundant set of the GenBank, EMBL and DDBJ database sequences) were conducted to confirm the total gene specificity of the nucleotide sequences chosen for the primers and to verify the absence of DNA polymorphisms. The nucleotide sequences of the primers used were as follows: Hs-ALB-U (5′-GCTGTCATCTCTTGTGGGCTGT-3′), Hs-ALB-L (5′-ACTCATGGGAGCTG CTGGTTC-3′), Total-JUN-U (5′-CACGGCCAACATGCTCAGG-3′) and Total-JUN-L (5′-GCATGAGTTGGCACCCACTGT-3′). The thermal cycling conditions included an initial denaturation step at 95 °C for 10 min and 50 cycles of 95 °C for 15 s and 65 °C for 1 min.

The results are presented as the N-fold difference in the specific human gene copy number (using Hs-ALB primers) relative to the sum of the mouse and human gene copy number (using Total-JUN primers), termed NHs/Total, which was determined with the following formula: NHs / Total = 2ΔCtsample. The ΔCt value of the sample was determined by subtracting the Ct value of the human gene from the Ct value of the total (mouse + human) gene. The NHs/Total values of the samples were subsequently normalized such that the median NHs/Total values for one human normal tissue were 100. As both ALB and JUN are present at a single copy in humans and in the mouse haploid genome, the final result (normalized NHs/Total value) indicates the proportion of human cells (in percentage) in a given PDOX tissue sample.

5.6. Measurement of plasma human interleukin-10 (IL-10)

Plasma samples were frozen within 6 h after sampling. Human IL-10 concentration in freshly thawed samples was measured using the cytometric bead array (CBA) technique (human IL-10 CBA kit; BD Biosciences, Le Pont-de-Claix, France) according to the manufacturer's recommendations, with a detection limit of 2.5 pg/ml. Blood samples were temporarily stored at −20 °C. IL-10 levels were determined in freshly thawed samples with the CBA technique (human IL-10 CBA kit; BD Biosciences™, Le Pont-de-Claix, France) according to the manufacturer's recommendations. Capture antibodies were mixed together in equal volumes: 50 µl of each sample and 50 µl of PE-conjugated detection antibody were added to 50 µl of a mixed-bead population. The mixture was incubated for 3 h at room temperature in the dark to form sandwich complexes. Then, the beads were washed with wash buffer, and data were acquired with a FACSCanto II flow cytometer (BD Biosciences). FACSDiva (v. 6·1·3) and FCAP software (v. 10·1) (BD Biosciences) were used for the analyses.

To correlate the tumor burden to the plasma IL-10 level, mouse blood samples were obtained every 15 days and at the time of sacrifice in the first PDOX-model.

5.7. Preclinical test

To test the suitability of PCNSL-PDOX models for preclinical experiments, we administered ibrutinib (30 mg/kg/day) or placebo by tube feeding for only 5 days (starting 49 days after inoculation of the tumor sample) to 6 mice bearing a PDOX-model harboring a mutation of CD79A and CD79 B. This experiment was not designed as a preclinical test of ibrutinib efficacy, but rather to illustrate the model's responsiveness to a short-term target therapy. Serum was collected 3 day before the start of Ibrutinib treatment and 4 h after the last ibrutinib administration, for measuring the IL-10 level. Mice were sacrificed at D53, 4 h after the last ibrutinib administration. At sacrifice, the brains were removed and fixed in 4% formalin. For each brain, four slices of 3 µm were obtained from 4 regions (at the site of inoculation, in the frontal lobe, in midbrain and cerebellum/brain stem) and each slice was evaluated for CD-20 expression. The proportion of CD20-stained cells was calculated by Aera Fraction, using Image J software. Pictures were acquired on motorized Axio Imager M2 Zeiss (objective x10). Image acquisition and image analysis were performed on workstations of the PICT-IBiSA Imaging facility of Institut Curie. Ibrutinib was provided by Pharmacyclics®.

5.8. Study approval

Animal experiments, care and housing were done in accordance with the institutional guidelines of the French Ethics Committee (Ministère de l'Alimentation, de l'Agriculture et de la Pêche, Direction de la Santé et de la Protection Animale, Paris, France), and the European Community (2010/63/UE) for the care and use of laboratory animals and under the supervision of authorized investigators. Experimental procedures were specifically approved by the ethics committee of the Institut Curie (CEEA-IC 2017-018) in compliance with the international guidelines.

Conflict of interest

No conflict of interest.

Acknowledgments

This work was funded by a grant from the National Institute for Cancer (Cancéropôle Ile de France, Emergence, EMERG-2, 2016), by Institut Curie Research Centre collaborative programs PIC3i, and by PRT-K 2017 1-RT-04 (DGOS et INCa).

Ibrutinib was provided by Janssen R&D, LLC, Spring House, PA. Janssen did not participate in the conception, conduction, or analysis of this work or in the writing of this report.

A special thanks to Beatrice Calandre for her logistic help with the CSF samples.

We acknowledge the PICT-IBiSA IBiSA Imaging facility of Institut Curie, Orsay member of the France-BioImaging national research infrastructure supported by the French National Agency (ANR-10-INSB-04, “Investments for the future”).

References

[1] S. Camilleri-Broët, E. Crinière, P. Broët, et al., A uniform activated B-cell-like immunophenotype might explain the poor prognosis of primary central nervous system lymphomas: analysis of 83 cases, Blood 107 (1) (2006) 190–196.
[2] M. Montesinos-Rongen, A. Brunn, S. Bentink, et al., Gene expression profiling suggests primary central nervous system lymphomas to be derived from a late germinal center B cell, Leukemia 22 (2008) 400–405.
[3] A. Gonzalez-Aguilar, A. Idbaih, B. Boisselier, et al., Recurrent mutations of MYD88 and TBL1XR1 in primary central nervous system lymphomas, Clin. Cancer Res. 18 (19) (2012) 5203–5211.
[4] B. Chapuy, M.G. Roemer, C. Stewart, et al., Targetable genetic features of primary testicular and primary central nervous system lymphomas, Blood 127 (7) (2016) 869-8.
[5] H.W. Tun, D. Personett, K.A. Baskerville, et al., Pathway analysis of primary central nervous system lymphoma, Blood 111 (6) (2008) 3200–3210.
[6] M. Krumbholz, D. Theil, T. Derfuss, et al., BAFF is produced by astrocytes and up-regulated in multiple sclerosis lesions and primary central nervous system lymphoma, J. Exp. Med. 201 (2) (2005) 195–200.
[7] L.L. Muldoon, C. Soussain, K. Jahnke, et al., Chemotherapy delivery issues in central nervous system malignancy: a reality check, J. Clin. Oncol. 25 (16) (2007) 2295–2305 (Review).
[8] A.J. Ferreri, K. Cwynarski, E. Pulczynski, et al., Chemoimmunotherapy with methotrexate, cytarabine, thiotepa, and rituximab (MATRix regimen) in patients with primary CNS lymphoma: results of the first randomisation of the international

extranodal lymphoma study group-32 (IELSG32) phase 2 trial, Lancet Haematol. 3 (5) (2016) e217–e227.
[9] A. Omuro, D.D. Correa, L.M. DeAngelis, et al., R-MPV followed by high-dose chemotherapy with TBC and autologous stem-cell transplant for newly diagnosed primary CNS lymphoma, Blood 125 (9) (2015) 1403–1410.
[10] C.P. Hans, D.D. Weisenburger, T.C. Greiner, et al., Confirmation of the molecular classification of diffuse large B-cell lymphoma by immunohistochemistry using a tissue microarray, Blood 103 (1) (2004) 275–282.
[11] T.X. Lu, Y. Miao, J.Z. Wu, et al., The distinct clinical features and prognosis of the $CD10^{+}MUM1^{+}$ and $CD10^{-}Bcl6^{-}MUM1^{-}$ diffuse large B-cell lymphoma, Sci. Rep. 6 (2016) 20465.
[12] L. Nguyen-Them, M. Costopoulos, M.L. Tanguy, et al., The CSF IL-10 concentration is an effective diagnostic marker in immunocompetent primary CNS lymphoma and a potential prognostic biomarker in treatment-responsive patients, Eur. J. Cancer 61 (2016) 69–76.
[13] C. Grommes, A. Pastore, N. Palaskas, et al., Ibrutinib unmasks critical role of Bruton tyrosine kinase in primary CNS lymphoma, Cancer Discov. 7 (9) (2017) 1018–1029.
[14] U. Ben-David, G. Ha, Y.Y. Tseng, et al., Patient-derived xenografts undergo mouse-specific tumor evolution, Nat. Genet. 49 (11) (2017) 1567–1575.
[15] L. Zhang, K. Nomie, H. Zhang, T. Bell, L. Pham, S. Kadri, J. Segal, S. Li, S. Zhou, D. Santos, S. Richard, S. Sharma, W. Chen, O. Oriabure, Y. Liu, S. Huang, H. Guo, Z. Chen, W. Tao, C. Li, J. Wang, B. Fang, J. Wang, L. Li, M. Badillo, M. Ahmed, S. Thirumurthi, S.Y. Huang, Y. Shao, L. Lam, Q. Yi, Y.L. Wang, M. Wang, B-cell lymphoma patient-derived xenograft models enable drug discovery and are a platform for personalized therapy, Clin. Cancer Res. 23 (15) (2017 Aug 1) 4212–4223.
[16] A. Rotolo, V.S. Caputo, M. Holubova, N. Baxan, O. Dubois, M.S. Chaudhry, X. Xiao, K. Goudevenou, D.S. Pitcher, K. Petevi, C. Kachramanoglou, S. Iles, K. Naresh, J. Maher, A. Karadimitris, Enhanced anti-lymphoma activity of CAR19-iNKT cells underpinned by dual CD19 and CD1d targeting, Cancer Cell 34 (4) (2018 Oct 8) 596–610.
[17] X. Wang, C. Huynh, R. Urak, M. Walter, L. Weng, L. Lim, V. Vyas, B. Aguilar, A. Brito, A. Sarkissian, A. Bandara, E. Budde, L. Popplewell, T. Tanya Siddiqi, C. Brown, S. Forman, The Cerebroventricular Environment Reprograms Locally Infused CAR T Cells for Superior Activity Against Both CNS and Systemic B Cell Lymphoma, ASH meeting, San Diego, CA, 2018 (Abstr # 965).
[18] A.M. Bolger, M. Lohse, B. Usadel, Trimmomatic: a flexible trimmer for Illumina sequence data, Bioinformatics 30 (15) (2014) 2114–2120.
[19] A. McKenna, M. Hanna, E. Banks, et al., The genome analysis toolkit: a MapReduce framework for analyzing next-generation DNA sequencing data, Genome Res. 20 (9) (2010) 1297–1303.
[20] K. Wang, H. Hakonarson, ANNOVAR: functional annotation of genetic variants from high-throughput sequencing data, Nucleic Acids Res. 38 (16) (2010) e164.
[21] A.L. Ramos, L. Lichtenstein, M. Gupta, et al., Oncotator: cancer variant annotation tool, Hum. Mutat. 36 (4) (2015) E2423–E2429.
[22] A. Mayakonda, D.C. Lin, Y. Assenov, C. Plass, H.P. Koeffler, Maftools: efficient and comprehensive analysis of somatic variants in cancer, Genome Res. 28 (11) (2018) 1747–1756.
[23] N.L. Bray, H. Pimentel, P. Melsted, L. Pachter, Near-optimal probabilistic RNA-seq quantification, Nat. Biotechnol. 34 (5) (2016) 525–527.
[24] D.A. Bolotin, S. Poslavsky, I. Mitrophanov, et al., MiXCR: software for comprehensive adaptive immunity profiling, Nat. Methods 12 (5) (2015) 380–381.
[25] M. Shugay, D.V. Bagaev, M.A. Turchaninova, et al., VDJtools: unifying post-analysis of T cell receptor repertoires, PLoS Comput. Biol. 11 (11) (2015) e1004503.